Carbon 146 (2019) 438–446

Contents lists available at ScienceDirect

Carbon

journal homepage: www.elsevier.com/locate/carbon

Laser-driven proliferation of sp^2-sp^3 changes during anti-Stokes white light emission of μ-diamonds

Adam Olejniczak [a, *], Robert Tomala [a], Bartłomiej Cichy [a], Paweł Głuchowski [a], Marcin Jakimów [b], Aneta Zięba [b], Leszek Kępiński [a], Oleg Ignatenko [c], Wiesław Stręk [a, **]

[a] Polish Academy of Sciences, Institute of Low Temperatures and Structural Research, 50-422, Wroclaw, Poland
[b] Nanores Sp. Z o. o. Sp. K., Ul. Bierutowska 57-59, 51-317, Wrocław, Poland
[c] Scientific-Practical Material Research Center of the National Academy of Sciences of Belarus, Brovki 19, 220072, Minsk, Belarus

ARTICLE INFO

Article history:
Received 30 November 2018
Received in revised form
1 February 2019
Accepted 7 February 2019
Available online 12 February 2019

ABSTRACT

The paper presents the investigations of laser-induced white light emission (LIWE) and structural changes in diamonds after continuous wavelength near infrared laser excitation. Micro-size diamonds were synthesized using high pressure high temperature method and then excited using continuous wavelengths near infrared (808, 975, 1064 nm) laser diodes in vacuum. The structure and morphology of the samples were investigated before and after laser excitation using XRD, Raman spectroscopy and SEM/FIB and TEM microscopy. Broadband, intense, anti-Stokes LIWE with very low threshold were observed. LIWE resulted in the graphitization of the diamond grain surface with different stages of graphitization depending on the excitation time. A model of an sp^2-sp^3 hybridization switch process assisting the multiphoton ionization and free to bound recombination of electron between two carbon atoms were proposed.

1. Introduction

Since the first report on the possibility of broadband, anti-Stokes, laser-induced white light emission (LIWE) generation from lanthanide-compounds by Wang and Tanner [1], extensive research on this phenomenon has been continued. Broadband emission from lanthanide-oxides (Yb_2O_3, Sm_2O_3 and CeO_2) induced by continues wavelength (CW) 975 nm laser excitation in vacuum was first explained in terms of multiphoton absorption and upconverting luminescence. A large number of matrices were examined as materials for LIWE generation, i.e. $LiYbP_4O_{12}$ [2], YAG [3], Er_2O_3 [4], $Y_2Si_2O_7$ [5], $NdAlO_3$ [6], $LiYbF_4$ [7] or Sr_2CeO_4 [8]. LIWE was found to be a threshold phenomenon. It depends non-linearly on the excitation power ($I \sim P^N$), where N is interpreted as a process order parameter associated with the number of absorbed photons. Long build-up and decay times are distinctive as well as an emission decrease with increasing pressure. The intervalence charge transfer (IVCT) model proposed by Seijo and Barandiran [9,10] was applied to explain the LIWE observed in Sr_2CeO_4. It describes the creation of coupled pairs of Ce^{3+}-Ce^{4+} ions and the multiphoton absorption and broadband emission as the diabatic process of valency change in ion pairs.

The recent experiments of Strek et al. have shown intense, anti-Stokes LIWE from graphene-based materials, i.e. graphene ceramics [11] and graphene foam [12] after the excitation of samples with a CW laser from the near infra-red (NIR) range. It is particularly interesting since all materials for which LIWE was observed previously were large bandgap insulators. For graphene with a zero bandgap, it is relatively easy to excite and even fully ionize the electron from the valence band. The relaxation of the ionized electron can lead to the sp^2 to sp^3 hybridization change and induce the structural disorder of graphene and form local defect states. Because graphene ceramics and graphene foam are initially highly disordered and defected materials, the sp^2 to sp^3 hybridization change can be achieved even more easily [13,14]. Olejniczak et al. [15] investigated the light-induced confinement of electrons in disordered graphene layers resulting in absorption and emission in the visible and NIR spectrum. Due to intense optical excitation, a large number of electrons can be ionized simultaneously in an avalanche process resulting in the distortion of the graphene electronic ground state and the formation of the plasma region near

* Corresponding author.
** Corresponding author.
E-mail addresses: a.olejniczak@intibs.pl (A. Olejniczak), w.strek@intibs.pl (W. Stręk).

https://doi.org/10.1016/j.carbon.2019.02.020
0008-6223/

the sample's surface [12]. A highly disturbed graphene structure can reach the false ground state with a completely new geometrical arrangement. A semiconducting phase with mixed sp^2/sp^3 hybridization called diaphite [16–18] was proposed to be formed in graphene ceramics during the LIWE process. It was shown, that laser-induced structural changes (hybridization changes) in graphene can proliferate in the sample to form larger structures. The excitation of only few atoms in a graphene bilayer can result in the formation of a larger number of interlayer bonds in a cooperative process [19,20]. The already existing small sp^3-bonded domains can easily merge during the lattice relaxation and stabilize as large structures [21].

Such structural changes were not observed in the previously investigated lanthanide compounds due to a large bandgap and the difficulty in ionizing a large number of electrons. Moreover, the remarkable feature of the carbon element is the ease of forming a number of various allotropic forms differing in structural and electronic properties [22]. Despite strong differences in physical properties between two extreme cases of carbon allotropes – fully sp^2-bonded graphite and fully sp^3-bonded diamond structures, the total energy of diamond structure is only 0.02 eV/atom higher than for graphite structure [23]. On the other hand, the energy barrier of graphite to diamond conversion is equal to 0.33 eV/atom [24]. Considering the electronic structure of the materials, diamond being a wide bandgap semiconductor is similar to previously investigated lanthanide-oxides, however, the charge-transfer processes are unlikely due to the covalent nature of the carbon-carbon bonds in the diamond structure. Recently, however, the bright, anti-Stokes, LIWE from micrometer-sized diamonds (μ-diamonds) were reported by Strek et al. [25].

The subject of this work was then to investigate the possibility of generating LIWE from the diamond as well as the laser-induced sp^2-sp^3 structural changes in the diamond structure. Due to the wide bandgap of pure diamond, a large amount of energy should be applied to ionize an electron from the valence band. For this study, high pressure high temperature (HPHT) produced micrometer-sized diamonds were investigated. The HPHT method was successful as regards synthesis, however, produced diamond crystals were characterized by a large number of impurities coming from the catalyst, nitrogen or vacancies. Moreover, because of the micrometer size of the produced diamonds, the large surface introduces a considerable number of defect states originating from the surface reconstruction. Such defects could mediate in the process of electron ionization facilitating the white-light emission generation. Detailed analysis of the structure of a sample before and after laser treatment is presented. The theoretical model of laser-induced structural changes in diamond, assisting multi-photon ionization and anti-Stokes white light emission, is proposed.

2. Experimental

The micrometer-sized diamond crystals were synthesized using the HPHT sintering technique. The alloy of nickel and manganese was used as a catalyst to reduce the pressure and temperature of crystallization. The catalyst and graphite (GMZ-OCCH) powder were stirred for 20 h. The reaction mixture was pressed at 0.2 GPa in a form of 12 mm diameter and 10 mm height. The diamonds were synthesized by sintering of the obtained green body at 5 GPa and 1500 °C.

LIWE spectra were measured at low pressure condition using the vacuum cell supplied with Turbomolecular Drag Pump TMH071P and an electronic drive unit TC 600 (Pfeiffer). The value of dynamic vacuum was constant during experiment and it was 10^{-5} hPa. The laser diodes (LD) operating at 808 nm, 975 nm and 1064 nm CW LD 2.0 W (CNI Lasers) and AVS-USB2000 Spectrometer (Avantes) were used as an excitation source and a detection system, respectively. The lasing threshold of the used laser diodes was about 400 mA. The numerical aperture of the optical fiber (Ocean Optics) collecting white light emission was 0.22. The laser beam was focused on the sample using glass lens with focal length 40 mm. The size of the laser beam focused on the sample was dependent on excitation wavelength and it was 140–190 μm, so the power density for 1 W excitation is ~4400 W/cm^2. The absorption spectra were measured using Varian Cary 5E UV-VIS-NIR spectrophotometer in the reflection mode, and Al_2O_3 powder was used as the reference. Fig. S1 in the Supplementary Information (SI) presents the scheme of the experimental setup of LIWE generation.

The scanning electron microscopy (SEM) was utilized for the investigation of the size and morphology of the crystals, and the Focused Ion Beam (FIB) cross-sections were also made using a dual beam SEM/Ga-FIB FEI Helios NanoLab 600i microscope. X-ray powder diffraction (XRD) studies were carried out on a PANalytical X'Pert Pro diffractometer (Cu Kα1: 1.54060 Å). The Raman measurements were performed in back-scattering geometry using a Renishaw InVia Raman microscope equipped with a confocal DM 2500 Leica optical microscope and a CCD detector. The Raman spectra were recorded under excitation with a diode laser emitting at a 514 nm and 20x LWD objective in a single scan with a 20 s exposure time in the spectral range 100–3300 cm^{-1}. The position of the Raman peaks was calibrated before data collection using an Si reference sample as an internal standard with the peak position at 520.3 cm^{-1}. Transmission Electron Microscopy (TEM) measurement was made with a Philips CM-20 SuperTwin TEM microscope, operating at 160 kV. Thin lamella with thickness below 100 nm was cut out from a sample using Ga–FIB microscope and was mounted on the copper TEM grid. Bright field and selected area electron diffraction (SAED) patterns were acquired on Gatan Orius CCD camera and were analyzed with Gatan DigitalMicrograph software.

All calculations were performed within the density functional theory using the GAMESS-US package. The B3LYP exchange-correlation functional and 6-31G(d) basis set were used. The self-consistent field convergence threshold was set to 10^{-5} Ha, and geometry optimization threshold was $5{\cdot}10^{-4}$ Ha/Bohr. Four diamond clusters of octahedral shapes with different sizes (35, 84, 165, 286 carbon atoms) and three clusters of truncate octahedron shapes (66, 123, 208 carbon atoms) were cut out from a bulk diamond structure and all dangling bonds on the surface were passivated with hydrogen atoms to obtain a full sp^3 structure. The geometry of all clusters was optimized and the electronic structure was calculated. Ionization potential (*IP*) was calculated for every cluster according to the equation:

$$IP = E_{n-1} - E_n. \quad (1)$$

Where E_n and E_{n-1} are total energies of an optimized diamond cluster, and the cluster optimized after removing of 1 electron. Defected clusters were prepared by removing hydrogen atoms from the diamond surface (Fig. S31 in SI). In the case of octahedral clusters, 2, 4 and 6 hydrogen atoms were removed from the same (111) surface to reveal 2, 4 and 6 carbon atoms, respectively. For truncated octahedron clusters, 8 hydrogen atoms were removed from the same (100) surface to reveal 4 carbon atoms. The geometry of the defected clusters was optimized and electronic structure was calculated.

3. Results and discussion

The μ-diamonds sample was excited using 808 nm, 975 nm, or 1064 nm laser diode and for each case the broadband, intense white

light emission was observed. Representative white light emission spectra are presented in Fig. 1a. One may see, that the emission band maximum is blue shifted with increasing excitation wavelengths. Fig. S3 in SI depicts the position of the emission maximum as obtained from the Gaussian fitting of the emission spectra. It is worth noting that such a shift of the white-light emission maximum for different excitation wavelengths was not observed in previous graphene or lanthanide samples [7,11,12] and will be further examined in our future works. The intensity of LIWE scales with excitation power like P^N. Fig. 1b presents the dependence of the normalized integrated LIWE intensity as a function of the excitation power for different excitation wavelengths. The threshold of LIWE is much lower comparing to other materials and bright, white light emission was clearly visible just above the LD laser action threshold. The image of the observed white light emission and CIE chromaticity coordinates are presented in Fig. S1 and Fig. S4 in SI, respectively. It has to be pointed out that the measured μ-diamonds sample was a very loose material. During the high power laser excitation (ca. 1.2–1.5 W) it was observed that some diamond grains were pushed out from the focal plane. This phenomenon suggests that the laser-induced ionization takes place and the electrons are accumulated on the grain's surface. If the excitation power exceeds a certain value, the number of electrons accumulated at the surface of a few neighboring μ-diamonds is large enough for the electrostatic repulsion force to push out the μ-diamonds from the focal plane. After the measurement, the blackening of the sample in the place of laser beam focusing was observed. Initially it was interpreted as a structural modification of the diamond structure, and the sample modified with focused 975 nm laser beam was selected for further investigation. The color of the sample after intense laser treatment was blackish (black sample in the following sections of the text), while the sample before the laser treatment was dark green (green sample in the following sections of the text), which can be clearly seen in Fig. S5 in Supplementary Information. Fig. S6 in SI shows the absorption spectra of the microdiamond sample before and after 975 nm laser treatment. The scanning electron microscope (SEM) analysis of the samples before and after laser treatment was performed and is presented in Fig. 2. It can be seen that the green sample (Fig. 2a) consists of grains of about 100 μm size. The grains with well-formed shapes (such as octahedrons and truncated octahedrons) as well as the grains with only some well-formed facets and others

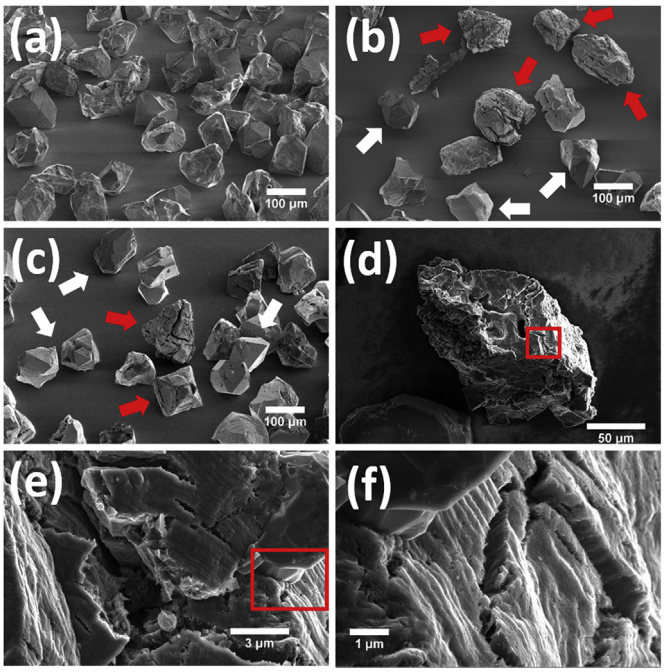

Fig. 2. (a) Representative SEM image of the green μ-diamond sample. (b,c) Representative SEM images of the black μ-diamond sample. Red arrows indicate diamond grains modified after focused laser beam treatment and white arrows – the unmodified ones. (d) SEM image of burned diamond grain with subsequent close-ups (e and f) of its surface. (A colour version of this figure can be viewed online.)

very deformed can be found in the sample (see Figs. S7–S10 in SI). Fig. 2b–f presents the representative SEM images of the black sample. Highly defected grains with a lot of cracks among the unmodified grains are clearly visible, which can be interpreted as the effect of laser modification. Despite the change of the sample color to blackish after laser treatment, only some grains differ from those in the green sample. Additional SEM images of black diamond grains are presented in SI, Figs. S11–S24. To obtain a better insight into the structure of laser beam modified diamond grains, XRD and Raman measurements were performed. The results of XRD measurements for green and black diamonds are presented in Fig. 3a and Fig. 3b, respectively. For the green sample only peaks

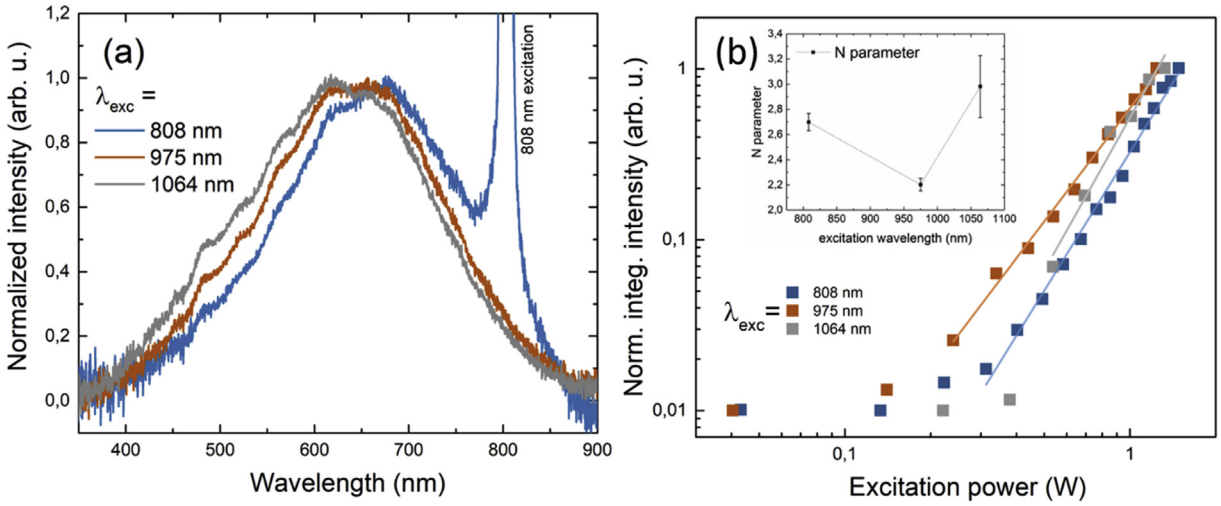

Fig. 1. (a) Normalized white light emission spectra for different excitation wavelengths. (b) Normalized integrated white light emission intensity as a function of excitation power for different excitation wavelengths. The inset shows values of parameter N obtained from linear fit. (A colour version of this figure can be viewed online.)

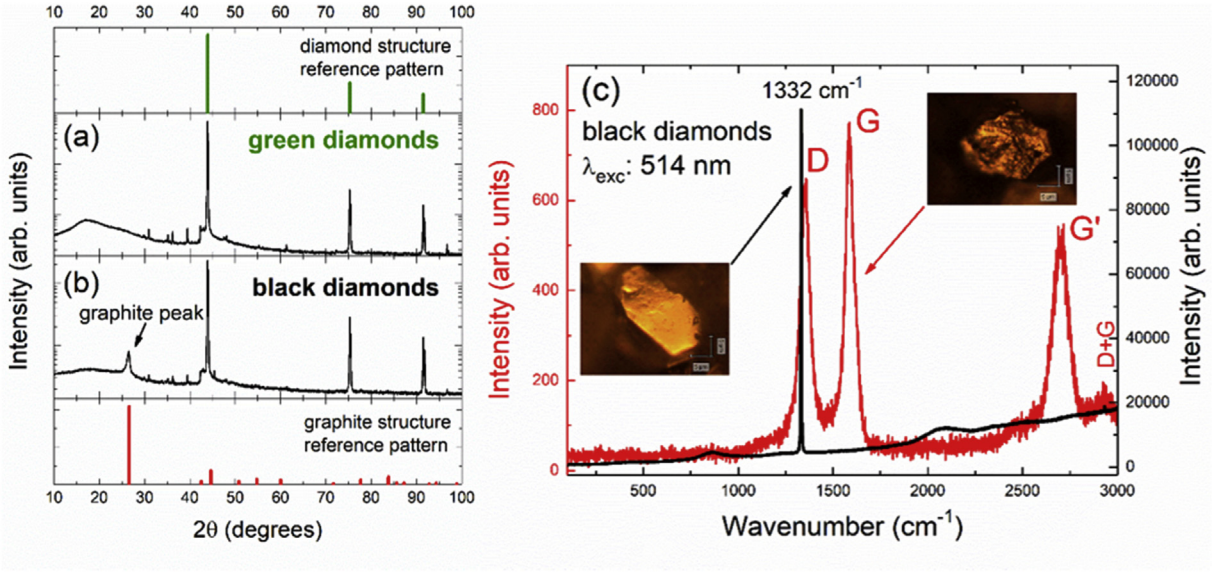

Fig. 3. XRD powder diffraction patterns of (a) green and (b) black μ-diamonds. The reference patterns for pure diamond and graphite structures are shown in the upper and lower part of the graph, respectively. (c) Raman spectra of laser modified (red curve) and unmodified (black curve) diamonds from black sample. The insets show microscope images of investigated μ-diamonds. (A colour version of this figure can be viewed online.)

originating from pure diamond structure are clearly visible, but for the black sample another peak originating from the graphite structure is also visible. It indicates the graphitization of the μ-diamond grains during the focused laser beam treatment. However, the small intensity of graphite peak is well rationalized since only some of the diamond grains were graphitized and the majority of them remained unchanged during the laser treatment. The peaks in the range of 30–40° can originate from various nitrogen [26,27] or metal [28,29] impurities.

During the powder XRD measurement the signal is collected from the ensemble of μ-diamonds, however, during the Raman measurement it was possible to focus on a single grain and distinguish between modified and unmodified grains. Fig. 3c presents the Raman spectra of laser modified and unmodified μ-diamonds from the black sample. It can be seen that unmodified grains (black curve) show only one Raman peak originating from the sp^3-bonded structure at 1332 cm^{-1} characteristic of diamonds [30], which also remains in harmony with the Raman spectra of the green diamonds sample (see Fig. S30 in SI).

The Raman spectrum of the laser-modified μ-diamond from the black sample is presented as the red curve in Fig. 3c. The peaks characteristic of a graphite structure centered at 1350 cm^{-1} (D band), 1582 cm^{-1} (G band), 2700 cm^{-1} (G′ band) and 2950 cm^{-1} (D + G band) are clearly observed [31]. G band originates from doubly degenerated phonon mode with the E_{2g} symmetry at Γ point of the Brillouin Zone for carbon sp^2 networks [32]. Also all kinds of graphitic materials exhibit G′ band as the overtone of D band. The intensity ratio of G and G' bands can determine the number of graphite layers. For a single graphene layer, the $I_{G'}/I_G \sim 2$ and it decreases with an increase in the number of layers [33]. In the case of laser modified μ-diamonds one may see that multi-layer graphite was obtained. D band is associated with graphite edges and it indicates the presence of defects in the graphite structure. It is not observed for highly crystalline samples. The D band to G band intensity ratio can be used to characterize the defect quantity of the graphitic sample [31]. Since D band intensity is almost as high as G band, the laser-modified μ-diamonds are characterized by a large number of defects and disorder, which can be also seen in the SEM images of laser-modified grains. D + G band at 2950 cm^{-1} is also induced by disorder [31]. Regarding the presented experimental results, it was concluded that the CW IR laser induced structural transition from diamond to a graphite structure was obtained.

It has to be pointed out that even after long excitation time, only some part of the total amount of diamond grains was modified. It can be concluded that only diamonds occurring at the focal point of the lens focusing the laser beam were modified. Even with long excitation time and mixing of the grains during the experiment, it was impossible to obtain the graphitization of the whole sample. Different stages of grain modification were observed during the SEM imaging of the sample.

One may find graphitized μ-diamonds which preserved their very symmetrical shape they had before laser treatment (Fig. 4a and b). The grains with graphitized (showing large number of cracks), but still very flat surface can also be found (Figs. 4c and 5a). These diamonds seem to be the most solid ones among other types of diamonds. The SEM images allow to surmise that the graphitization process did not reach the whole grain volume and only its surface was modified. Indeed, on the Focused Ion Beam cross section of the laser modified diamond grain (Figs. S27 and S28 in SI) one can see that structural defects and ruptures reach only the depth of few micrometers. Additionally, after removing the upper, laser-modified layer of the grain, it can be seen that the deeper parts of the grains are etched by the ion beam in a typical way showing characteristic ripples. Such ripples were observed previously by other groups [34,35] and also in our case during the FIB cross sectioning of the unmodified diamond grains (Figs. S25 and S26 in SI). The second type are highly modified μ-diamond grains characterized by numerous cracks (Fig. 4d,e,f) and stratifications without any symmetrical shape. For these grains the graphitization occurred at the deeper level, including the possible structural transformation of the whole grain. The destruction of some modified μ-diamonds was observed, which confirmed that the graphitization can occur for the whole grain volume (Fig. 4g,h,i).

It can be concluded that the graphitization is a time-dependent process which does not take place immediately for the whole grain volume. After some time spent in the focal plane of the laser beam, the grain's surface can be graphitized. The process still needs more time to proliferate to reach the whole volume of the grain. The

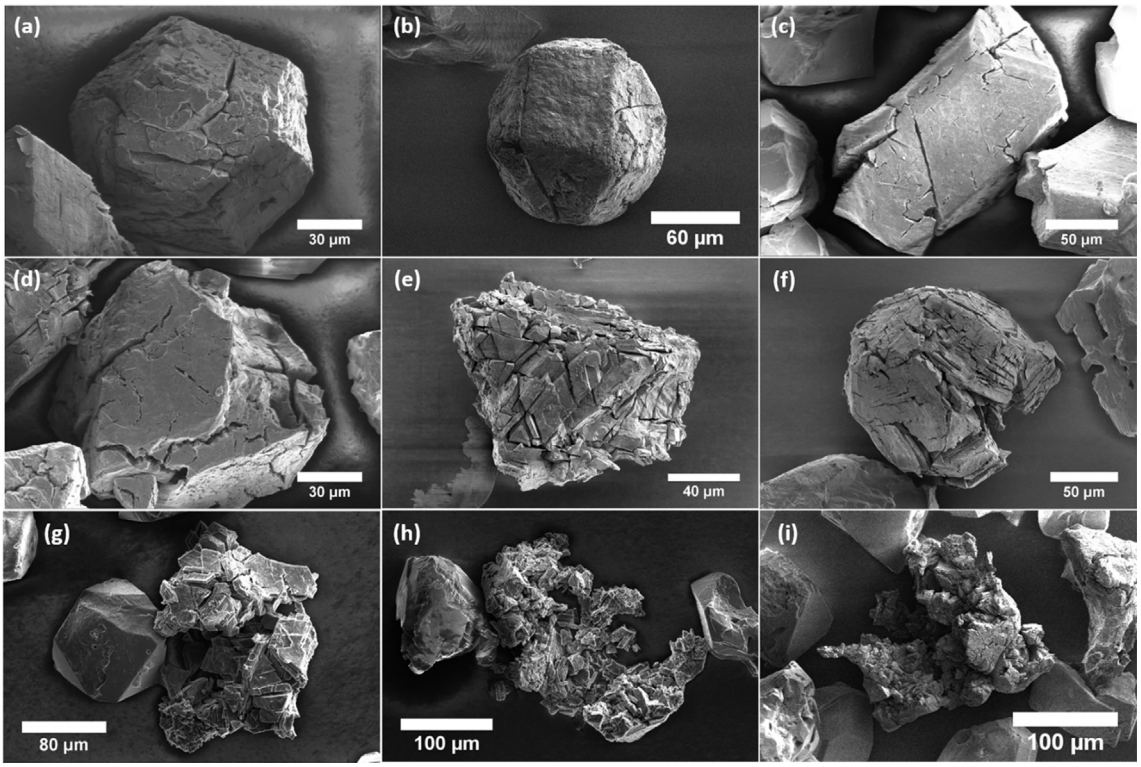

Fig. 4. SEM images of laser-modified μ-diamonds of various types. (a,b) Graphitized μ-diamonds, which preserved their very symmetrical shape. (c) Diamond grain with graphitized, but still very flat surface. (d,e,f) Highly modified grains with numerous cracks and without symmetrical shape. (g,h,i) Fully graphitized diamond grains.

presence of diamonds at different stages of the graphitization process originates from the electrostatic repulsion of grains after laser ionization of the grain's surface, pushing grains out of the focal plane of the laser beam, which was described earlier. Because the graphitized grains with very symmetrical shape and without any symmetry can be found in the black diamond sample simultaneously, it can be concluded that laser-induced graphitization process does not depend on initial crystallization quality and shape of individual grains.

To further characterize the proliferation of structural changes in diamonds a TEM measurement was made for a partially graphitized diamond. A thin lamella was prepared from a diamond with flat surface but with clearly visible cracks and defects indicating partial graphitization (Fig. 5a). Detailed process of lamella preparation is presented in Fig. S29 in Supporting Information. SEM image of the prepared lamella (Fig. 5b) shows two phases with noticeable contrast difference what was interpreted as a graphite (upper phase) and diamond (lower phase). Fig. 5c shows bright field TEM image of a boundary between intact (diamond) and transformed (graphitized) part of individual microdiamond. Numerous defects (dislocations) are seen in the diamond part, especially at the boundary. The identification of the phases present was done using selected area electron diffraction patterns (Fig. 5d,e,f). SAED pattern from diamond region (Fig. 5d) could be indexed as crystalline diamond in [1 2 -5] orientation, while the pattern from graphite region, close to the boundary (Fig. 5e), as crystallite graphite in [1−2 1 1] orientation. SAED pattern obtained from the „graphitic" region more distant from the boundary with the diamond shows different, polycrystalline character (Fig. 5f).

One may conclude that the graphite structure is stabilized at the boundary by the diamond structure and remains crystalline. Far from the boundary, the graphite structure can freely relax all the stresses originating from the crystal lattice mismatch and the graphite phase becomes more polycrystalline due to the defects and cracking. It agrees well with Raman measurement of black diamond sample. Because only the surface of the sample was measured, the Raman spectra showed large D band intensity, which is not observed for highly crystalline samples.

The processes of laser-induced sp^3 to sp^2 hybridization change proliferation were reported previously. Depending on laser beam parameters, such as pulse duration, radiation intensity or wavelength, the results of diamond surface irradiation can be different: from the formation of micro/nano-regions with partially sp^2-bonding up to the complete diamond to graphite transformation [36]. Neff et al. [37] irradiated the single-crystal diamond plate with Ti:Sapphire 800 nm fs-pulses at different fluences focusing the laser beam inside the diamond at the depth of 70 μm. They observed the optical breakdown near the focal plane and the extension of the modified region toward the laser beam, the so called graphitization wave. The investigation of the graphitization wave propagation velocity inside the material showed that it is a threshold process varying with the laser pulse energy and the distance from the focal plane. The authors found that numerous cracks are generated at the boundary of the modified region initiating the local graphitization wave propagation. They established that when the inner graphitized volume increases, the thermodynamic equilibrium between carbon phases shifts until the full transformation of diamond into graphite becomes impossible. Rehman & Janulewicz [38] showed that after the irradiation of monocrystalline diamond plate with fs-pulses of 800 nm Ti:Sapphire laser, the so called laser-induced periodic surface structures (LIPSS) were obtained. A detailed analysis using electron microscopy techniques showed that laser-structured spots consist mostly of amorphous carbon with crystalline graphite dispersed in the amorphous matrix. The authors found that a very thin (*ca.* 0.5 μm) transition zone between the graphitic bottom of the amorphous

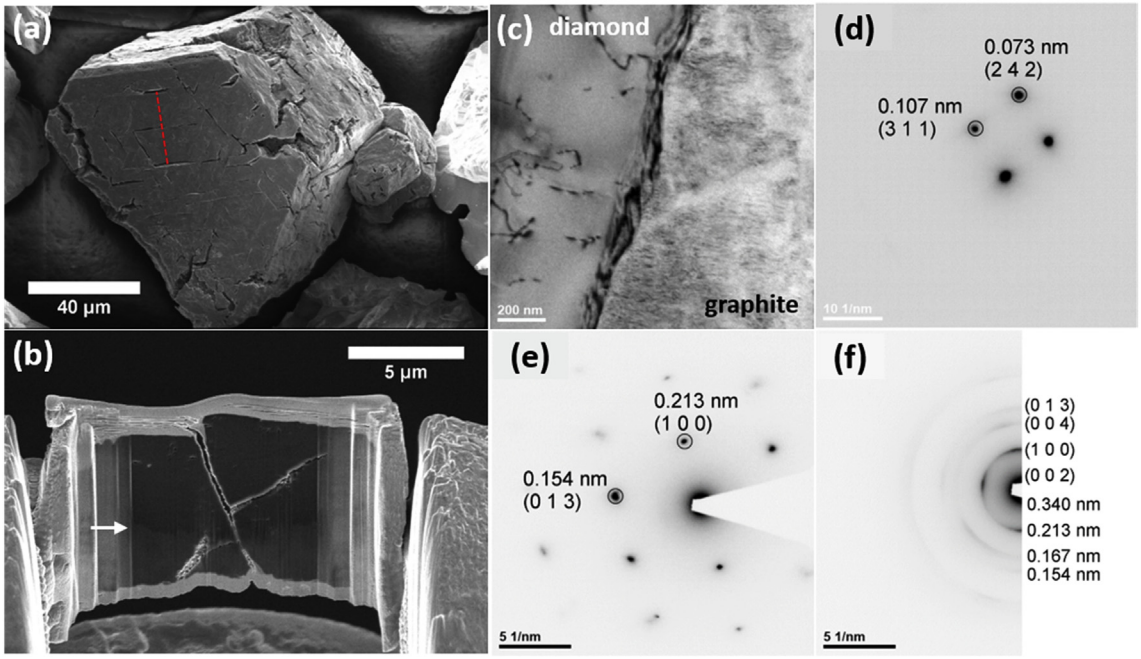

Fig. 5. (a) Graphitized µ-diamond chosen for lamella preparation. Red dotted line indicates the cracked place from where the lamella was cut out using SEM/Ga-FIB microscope. (b) SEM image of thin lamella. White arrow indicate the boundary between two phases with visible material contrast (c) TEM image of the boundary between diamond and graphite phases. (d) SAED pattern obtained from diamond region, (e) graphite region close to the boundary and (f) far from the boundary. (A colour version of this figure can be viewed online.)

layer and the pristine diamond substrate showed some rare cracks in the diamond crystal indicating the strong influence of the reaction shock generated in the material by such intense laser ablation. Calvani et al. [39,40] observed the LIPSS on the surface of polycrystalline CVD diamond plates irradiated with focused 800 nm fs-laser pulses in a high vacuum chamber for laser power density higher than the diamond ablation threshold. Laser modified diamond plates were characterized by over 90% absorptance from 200 nm up to 2 µm. A very high absorptance of these so called black diamond plates originated from the LIPSS since all residual graphitic-based content was removed in a strongly oxidizing solution after laser treatment, which was confirmed by Raman measurements.

On the other side, one may find a number of studies considering thermal graphitization of various diamond samples and the heating of the sample during CW IR laser excitation cannot be omitted. Yan et al. [41] investigated heat treatment of polycrystalline CVD diamond films within direct current arc plasma jest system up to 2000 °C. The macroscopic diamond to graphite phase transition, showing distinct graphite maximum on powder XRD pattern, occurred after heating of the sample to 1900 °C for 1 min. Also diamond band in the Raman spectra decreased significantly when the sample was heated to 1900 °C. Qian et al. [42] examined the thermal graphitization of micrometer-sized diamonds (30–40 µm) at different pressures. The volume percentage of graphite produced after annealing of diamonds at 2 GPa for 30 min was below 5% for 1300 K, and reached 20% at 1600 K. They showed, that with increasing of the diamond size, the graphitized volume percentage decreases. 20% of grain volume was graphitized after treatment of 30 µm sized diamonds with 1473 K for 30 min, when for 150 µm sized diamonds, the graphitized volume was below 5%. It can be seen that higher temperature and longer heating time (in order of minutes) is needed.

The temperature of the sample during LIWE generation can be estimated from the emission of Er^{3+}-doped $LiYbP_4O_{12}$ upconverting nanocrystalline sensors encrusted on the surface of the emitting sample. For graphene ceramics [11] the temperature of the sample was lower than 900 K for the highest excitation power (1.5 W). The sample temperature dependency on the excitation power density was measured for the Sr_2CeO_4 ceramics [8]. Temperature of the sample was about 500 K for power density equal to 5000 W/cm^2 and reached 1000 K at 7000 W/cm^2. For given excitation power densities (c.a. 4400 W/cm^2 at 1 W), we can estimate, that the temperature of the µ-diamonds is below 900 K. Because large amount of energy is utilized to generate and sustain LIWE, the heating of the sample is not sufficient to graphitize the sample only by temperature-driven process. Moreover, due to the ionization of the diamond surface and the electrostatic repulsion between grains is unlikely for single µ-diamond to maintain in to focal point of laser beam for several minutes.

The laser-driven graphitization of diamond was investigated theoretically by Strekalov et al. [43,44] who related it with the non-radiative electron-hole recombination processes. Graphitization initiates with the nucleation of a tiny graphite region in the focal point of laser beam causing the mechanical stress of the surrounding area. After the excitation pulse is over, graphitization should be accompanied by post-irradiation and accumulation effects.

The optical excitation of diamond requires a large amount of energy to transfer the electron from the valence to the conduction band, or to transfer the electron from one carbon atom to another via the ionization process (Fig. 6a). Such energy can be brought by UV excitation (e.g. using KrF excimer laser [45]) or during the multiphoton absorption process. Indeed the excitation of the sample during the laser-induced white light emission process was considered as multiphoton absorption process. Due to the large energy gap (5.4 eV), pristine diamond is transparent for a wide range of excitation, and so to excite the electron from the valence to the conduction band about 4–5 of 975 nm ($E_{ph} = 1.27$ eV) photons should be absorbed at the same time. Despite the fact that such

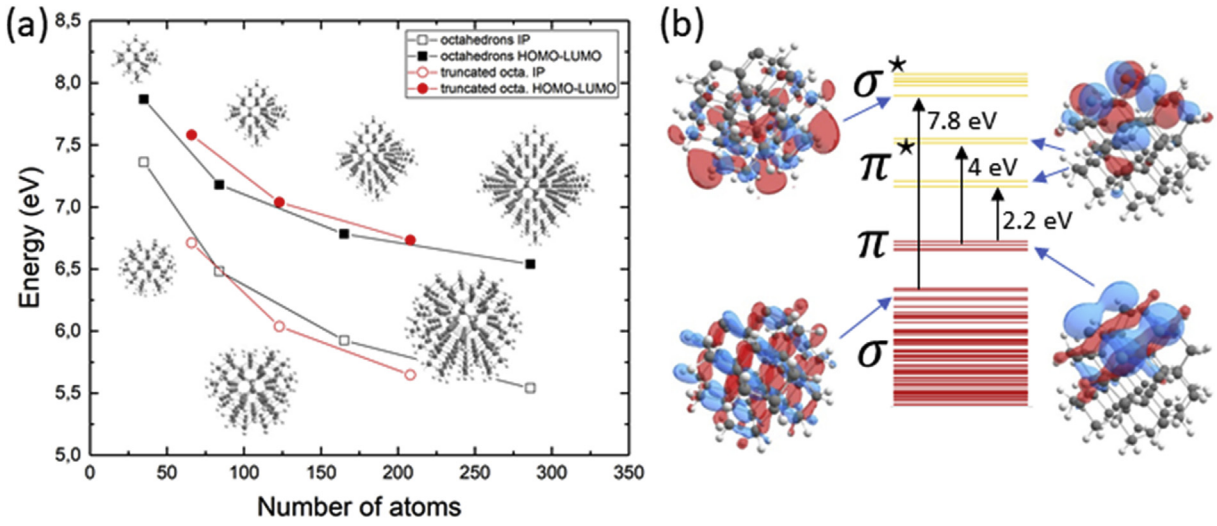

Fig. 6. (a) HOMO-LUMO energy gaps (full points) and the ionization potential (hollow points) of the model full-sp^3 diamond clusters as a function of size. Black points for octahedral clusters and red points for truncated octahedrons. (b) Electronic energy levels diagram of defected truncated octahedron diamond cluster with corresponding molecular orbitals. Fully occupied orbitals are given in red. The unoccupied ones – in yellow. (A colour version of this figure can be viewed online.)

high-order processes were reported previously [8,11], the simultaneous absorption of 5 photons seems to be less probable even for high excitation power.

However, if bulk diamond cannot be easily excited because of its large bandgap, it is possible to excite electrons from surface-originated defect states. As shown in Fig. 6b and Fig. S32, sp^3 to sp^2 hybridization change by surface reconstruction induces defect π and $\pi^\star$ electronic states in the diamond bandgap. Baitinger et al. [46] investigated the morphology of detonation nanodiamonds and found fullerene-like shell surrounding diamond nanocrystal core. Electronic bands of shell-structure consist of additional π and $\pi^\star$ between σ and $\sigma^\star$ diamond-like bands. To excite the electron from π to $\pi^\star$ states much less energy is needed, and the absorption of 2 or 3 photons would be sufficient, which is much more probable than the higher-order multiphoton absorption. Moreover, μ-diamonds obtained by the HPHT synthesis procedure are characterized by a large amount of impurities, such as nitrogen or metal (Fe, Ni) atoms built in the diamond structure. These impurities could also act as active sites for structural changes [47] and diamond cracking resulting in more defect states in the diamond bandgap. After the ionization of an electron from the diamond structure, it can be trapped by a defect state on the grain's surface. During the free to bound recombination process, electron emits light and, since the ionized free electrons can have any energy before the recombination, it results in the continuous spectra of emitted photons. The bound electron can be ionized again, due the strong excitation power density, and can recombine again with another surface trap emitting a photon. The proliferating ionization and recombination processes are shown schematically in Fig. S33. Long build-up times should be required for the electron plasma to obtain the equilibrium state between the ionization and recombination processes during LIWE and to fully return to the ground state after the end of laser excitation, which remains in agreement with the previous observations of Stręk et al. [25].

The ionization of an electron from the diamond structure can result in the C–C bond breaking and local sp^3 to sp^2 hybridization change and defect formation, whereas the recombination and trapping of the ionized electron in the surface trap state will result in the saturation of the dangling bond from the sp^2 carbon atom on the surface, and a local sp^2 to sp^3 transition. Such a process will last continuously during the laser excitation and each pair of ionization-recombination (ionization-trapping) action will be connected with the switch of the hybridization of the two carbon atoms. It can be presented graphically similarly as the IVCT mechanism of Ce^{3+}-Ce^{4+} ion pairs in the LIWE phenomenon in Sr_2CeO_4 [8]. Fig. 7a shows a schematic energy diagram of the hybridization switch assisted ionization and the (free-to-bound) recombination process. The breaking of the C–C bond and sp^3 to sp^2 hybridization change will result in the local defect π state formation. Due to the proliferation process and continuous ionization by strong laser excitation, the defects can group into a larger domain of sp^2-hybridized carbon atoms. A conceptual representation of such a situation is presented in Fig. 7b. The black curve in Fig. 7b represents the ground state potential energy surface during diamond to graphite transition. The values of energy barrier (0.33 eV/atom) and difference in total energy of graphite and diamond structures (0.02 eV/atom) were taken from Fahy et al. [24] Similar values for energy barrier were reported previously [48]. Blue parabolas represent the $\sigma^\star$ excited states. The electrons cannot be excited from the ground state directly to $\sigma^\star$ excited states because of the large energy gap in pristine diamond structure. However, for initially defected diamond structure, there are some π energy states in the bandgap and electron can be excited directly from this states. During the process of photoionization of the sample by intense, focused laser excitation, the sp^3 bonds can break and sp^2-hybridized defects are formed. The local ratio of sp^2/sp^3 hybridized carbon atoms will increase resulting in more defect π state formation, which will further facilitate ionization as an avalanche process. Finally, after crossing the transition energy barrier in the excited state, when local sp^2/sp^3 carbon atoms ratio approaches unity, the structure can collapse to the graphite domain and cause mechanical damage through structural tension.

4. Conclusions

The authors observed broadband, anti-Stokes and intense LIWE after excitation of HPHT-synthesized μ-diamonds with the near-infrared laser diodes. LIWE was characterized by a very low threshold and the dependence of the emission maximum on the excitation wavelengths. Further extend research of LIWE phenomenon from diamond is needed, as it can be applied as novel, broadband white light sources. Moreover, the possibility of LIWE

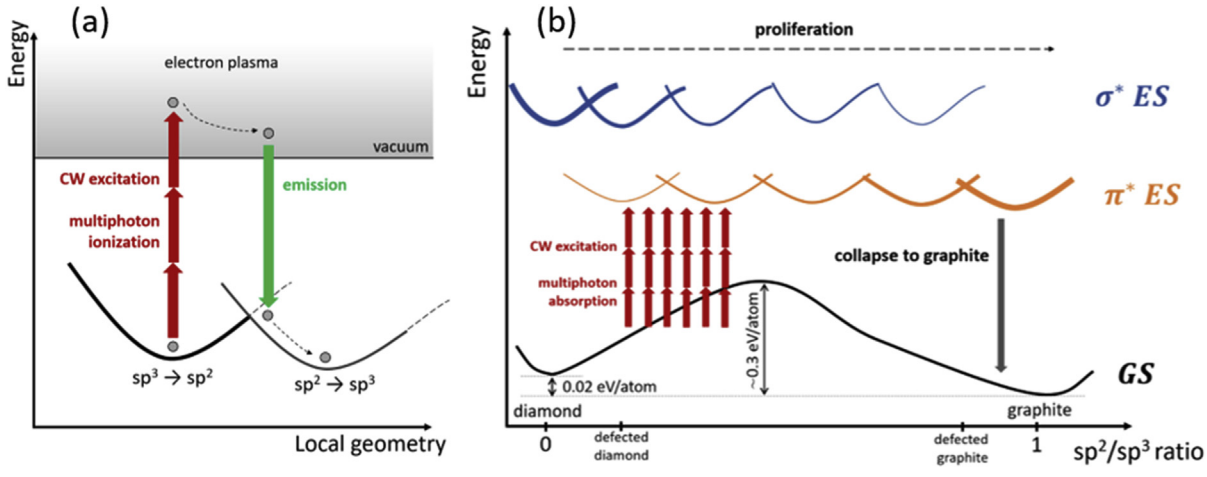

Fig. 7. (a) Schematic representation of the hybridization switch during the multiphoton ionization and free to bound recombination process. (b) Schematic representation of defect-states mediated diamond to graphite structural transformation. Black curve represents the ground state (GS) total energy per atom with indicated energy barrier and energy differences between diamond and graphite structures. Blue curves represents the $\sigma^{\star}$ excited states (ES) of sp^3 structure, and orange curves - $\pi^{\star}$ of sp^2 structure. (A colour version of this figure can be viewed online.)

modulation by modulation of the excitation laser beam can find the application in the technology of wireless communication between devices using visible light to transmit data, i.e. Li-Fi. Large ionizations of the grains' surface were observed for the highest excitation powers (ca. 1.2–1.5 W) resulting in the electrostatic repulsion of individual grains and pushing the grains out of the laser beam focal plane. The blackening of the sample was observed after laser treatment. The graphitization of μ-diamond grains was confirmed by XRD and Raman spectroscopy measurements and SEM/FIB imaging. Different stages of graphitization were observed, indicating that laser-induced diamond to graphite structural change rate depends on time during which an individual μ-diamonds grain remains in the laser beam focal point. The model of defect-mediated multiphoton electron ionization and free to bound recombination resulting in the continuous spectra of the emitted photons was presented. It was proposed that, similarly to IVCT mechanism, the sp^2-sp^3 hybridization switch of two carbon atoms occurs simultaneously with every ionization-recombination pair. Graphitization will occur when, due to proliferation, a certain number of sp^2-carbon defects near the diamond surface will group. Such an sp^2-defect group will spontaneously collapse to the graphite structure resulting in the surface tension and cracking of the grain.

Acknowledgements

This work was financed from the National Science Centre Poland within the OPUS 15 (2018/29/B/ST5/00819) grant. The numerical calculations presented in this work were performed using the Polish Grid (PLGrid) computational infrastructure. SEM imaging, FIB cross sectioning and TEM lamella preparation were done in Nanores Sp. z o. o. Sp. k. in Wrocław, Poland.

Appendix A. Supplementary data

Supplementary data to this article can be found online at https://doi.org/10.1016/j.carbon.2019.02.020.

References

[1] J. Wang, P.A. Tanner, Upconversion for white light generation by a single compound, J. Am. Chem. Soc. 132 (2010) 947–949.
[2] L. Marciniak, W. Strek, D. Hreniak, Y. Guyot, Temperature of broadband anti-Stokes white emission in LiYbP4O12: Er nanocrystals, Appl. Phys. Lett. 105 (2014) 1–5, https://doi.org/10.1063/1.4900965.
[3] J. Wang, J. Hua Hao, P.A. Tanner, Luminous and tunable white-light upconversion for YAG (Yb_3Al_5O_12) and (Yb,Y)_2O_3 nanopowders, Opt. Lett. 35 (2010) 3922, https://doi.org/10.1364/OL.35.003922.
[4] J. Wang, J.H. Hao, P.A. Tanner, Upconversion luminescence of an insulator involving a band to band multiphoton excitation process, Optic Express 19 (2011) 11753, https://doi.org/10.1364/OE.19.011753.
[5] R. Tomala, D. Hreniak, W. Strek, Influence concentration of Nd3+ion on the laser induced white emission of Y2Si2O7:Nd3+, Opt. Mater. 74 (2017) 135–138, https://doi.org/10.1016/j.optmat.2017.03.026.
[6] W. Strek, L. Marciniak, D. Hreniak, A. Lukowiak, Anti-Stokes bright yellowish emission of NdAlO3 nanocrystals, J. Appl. Phys. 111 (2012) 1–7, https://doi.org/10.1063/1.3674272.
[7] L. Marciniak, R. Tomala, M. Stefanski, D. Hreniak, W. Strek, Laser induced broad band anti-Stokes white emission from LiYbF4nanocrystals, J. Rare Earths 34 (2016) 227–234, https://doi.org/10.1016/S1002-0721(16)60018-2.
[8] W. Strek, R. Tomala, L. Marciniak, M. Lukaszewicz, B. Cichy, M. Stefanski, D. Hreniak, A. Kedziorski, M. Krosnicki, L. Seijo, Broadband anti-Stokes white emission of Sr $_2$ CeO $_4$ nanocrystals induced by laser irradiation, Phys. Chem. Chem. Phys. 18 (2016) 27921–27927, https://doi.org/10.1039/C6CP04904D.
[9] Z. Barandiarán, L. Seijo, Intervalence charge transfer luminescence: interplay between anomalous and 5 d - 4 f emissions in Yb-doped fluorite-type crystals, J. Chem. Phys. 141 (2014), https://doi.org/10.1063/1.4902759.
[10] L. Seijo, Z. Barandiarán, Intervalence charge transfer luminescence: the anomalous luminescence of cerium-doped Cs2LiLuCl6 elpasolite, J. Chem. Phys. 141 (2014), https://doi.org/10.1063/1.4902384.
[11] W. Strek, B. Cichy, L. Radosinski, P. Gluchowski, L. Marciniak, M. Lukaszewicz, D. Hreniak, Laser-induced white-light emission from graphene ceramics-opening a band gap in graphene, Light Sci. Appl. 4 (2015) e237, https://doi.org/10.1038/lsa.2015.10.
[12] W. Strek, R. Tomala, M. Lukaszewicz, B. Cichy, Y. Gerasymchuk, P. Gluchowski, L. Marciniak, A. Bednarkiewicz, D. Hreniak, Laser induced white lighting of graphene foam, Sci. Rep. 7 (2017) 1–9, https://doi.org/10.1038/srep41281.
[13] R.H. Telling, C.P. Ewels, A.A. El-Barbary, M.I. Heggie, Wigner defects bridge the graphite gap, Nat. Mater. 2 (2003) 333–337, https://doi.org/10.1038/nmat876.
[14] O. Leenaerts, B. Partoens, F.M. Peeters, Hydrogenation of bilayer graphene and the formation of bilayer graphane from first principles, Phys. Rev. B Condens. Matter 80 (2009) 1–6, https://doi.org/10.1103/PhysRevB.80.245422.
[15] A. Olejniczak, B. Cichy, L. Radosinski, W. Stręk, Light-induced confinement of electrons in stacked distorted graphene layers – (TD-)DFT study, Phys. Chem. Chem. Phys. (2017), https://doi.org/10.1039/C6CP07632G.
[16] J. Kanasaki, E. Inami, K. Tanimura, H. Ohnishi, K. Nasu, formation of sp3-bonded carbon nanostructures by femtosecond laser excitation of graphite, Phys. Rev. Lett. 102 (2009), 087402, https://doi.org/10.1103/PhysRevLett.102.087402.
[17] H. Ohnishi, K. Nasu, Photoinduced domain-type collective structural changes with interlayer σ-bonds in the visible region of graphite, Phys. Rev. B 79 (2009), 054111, https://doi.org/10.1103/PhysRevB.79.054111.
[18] L. Radosinski, F. Formalik, A. Olejniczak, A. Radosz, Diaphite, a new type of surface with mixed sp2-sp3hybridization for adsorption and functionalization, Appl. Surf. Sci. 404 (2017) 154–161, https://doi.org/10.1016/j.apsusc.2017.01.085.
[19] K. Nishioka, K. Nasu, Cooperative domain-type interlayer sp^3 -bond formation in graphite, Phys. Rev. B 82 (2010), 035440, https://doi.org/10.1103/

PhysRevB.82.035440.
[20] K. Nishioka, K. Nasu, Early-stage real-time dynamics of interlayer sp^3 -bond formation by visible-light irradiation of graphite, Phys. Rev. B 80 (2009), 235420, https://doi.org/10.1103/PhysRevB.80.235420.
[21] H. Ohnishi, K. Nasu, Generation and growth of sp3-bonded domains by visible photon irradiation of graphite, Phys. Rev. B 80 (2009), 014112, https://doi.org/10.1103/PhysRevB.80.014112.
[22] A. Hirsch, The era of carbon allotropes, Nat. Publ. Gr. 9 (2010) 868–871, https://doi.org/10.1038/nmat2885.
[23] S. Fahy, S.G. Louie, M.L. Cohen, Theoretical total-energy study of the transformation of graphite into hexagonal diamond, Phys. Rev. B 35 (1987) 7623–7626, https://doi.org/10.1103/PhysRevB.35.7623.
[24] S. Fahy, S.G. Louie, M.L. Cohen, Pseudopotential total-energy study of the transition from rhombohedral graphite to diamond, Phys. Rev. B 34 (1986) 1191–1199, https://doi.org/10.1103/PhysRevB.34.1191.
[25] W. Strek, A. Olejniczak, R. Tomala, B. Cichy, A. Zhaludkevich, A. Konovalova, O. Ignatenko, The bright white emission from μ -diamonds, Proc. SPIE 10683 (2018), 1068307.
[26] Y. Borzdov, Y. Pal'yanov, I. Kupriyanov, V. Gusev, A. Khokhryakov, A. Sokol, A. Efremov, HPHT synthesis of diamond with high nitrogen content from an Fe3N-C system, Diam. Relat. Mater. 11 (2002) 1863–1870, https://doi.org/10.1016/S0925-9635(02)00184-X.
[27] Z.Z. Liang, H. Kanda, X. Jia, H.A. Ma, P.W. Zhu, Q.F. Guan, C.Y. Zang, Synthesis of diamond with high nitrogen concentration from powder catalyst-C-additive NaN3 by HPHT, Carbon N. Y. 44 (2006) 913–917, https://doi.org/10.1016/j.carbon.2005.10.018.
[28] B. Xu, M. Sen Li, J.J. Cui, J.H. Gong, S.H. Wang, An investigation of a thin metal film covering on HPHT as-grown diamond from Fe-Ni-C system, Mater. Sci. Eng. 396 (2005) 352–359, https://doi.org/10.1016/j.msea.2005.02.005.
[29] Z.F. Zhang, X.P. Jia, S.S. Sun, X.B. Liu, Y. Li, B.M. Yan, H.A. Ma, Effects of hydrogen impurity on diamond crystal growth process, Int. J. Refract. Metals Hard Mater. 38 (2013) 111–117, https://doi.org/10.1016/j.ijrmhm.2013.01.009.
[30] S.A. Solin, A.K. Ramdas, Raman spectrum of diamond, Phys. Rev. B 1 (1970) 1687–1698, https://doi.org/10.1103/PhysRevB.1.1687.
[31] M.A. Pimenta, G. Dresselhaus, M.S. Dresselhaus, L.G. Cançado, A. Jorio, R. Saito, Studying disorder in graphite-based systems by Raman spectroscopy, Phys. Chem. Chem. Phys. 9 (2007) 1276–1291, https://doi.org/10.1039/b613962k.
[32] F. Tuinstra, J.L. Koenig, Raman spectrum of graphite, J. Chem. Phys. 53 (1970) 1126–1130, https://doi.org/10.1063/1.1674108.
[33] A.C. Ferrari, Raman spectroscopy of graphene and graphite: disorder, electron-phonon coupling, doping and nonadiabatic effects, Solid State Commun. 143 (2007) 47–57, https://doi.org/10.1016/j.ssc.2007.03.052.
[34] X. Ding, G.C. Lim, C.K. Cheng, D.L. Butler, K.C. Shaw, K. Liu, W.S. Fong, Fabrication of a micro-size diamond tool using a focused ion beam, J. Micromech. Microeng. 18 (2008), https://doi.org/10.1088/0960-1317/18/7/075017.
[35] D.P. Adams, M.J. Vasile, T.M. Mayer, V.C. Hodges, Focused ion beam milling of diamond: effects of H[sub 2]O on yield, surface morphology and microstructure, J. Vac. Sci. Technol. B Microelectron. Nanom. Struct. 21 (2003) 2334, https://doi.org/10.1116/1.1619421.
[36] V.I. Konov, Laser in micro and nanoprocessing of diamond materials, Laser Photon. Rev. 6 (2012) 739–766, https://doi.org/10.1002/lpor.201100030.
[37] M.N.T. V Kononenko, S.M.P. V Romano, W.L.V.I. Konov, Femtosecond Laser Writing of Buried Graphitic Structures in Bulk Diamond, 2009, pp. 543–547, https://doi.org/10.1007/s00339-009-5393-x.
[38] Z.U. Rehman, K.A. Janulewicz, Structural transformation of monocrystalline diamond driven by ultrashort laser pulses, Diam. Relat. Mater. 70 (2016) 194–200, https://doi.org/10.1016/j.diamond.2016.11.004.
[39] P. Calvani, A. Bellucci, M. Girolami, S. Orlando, V. Valentini, R. Polini, D.M. Trucchi, Black diamond for solar energy conversion, Carbon N. Y. 105 (2016) 401–407, https://doi.org/10.1016/j.carbon.2016.04.017.
[40] A. Bellucci, P. Calvani, M. Girolami, S. Orlando, R. Polini, D.M. Trucchi, Optimization of black diamond films for solar energy conversion, Appl. Surf. Sci. 380 (2016) 8–11, https://doi.org/10.1016/j.apsusc.2016.02.107.
[41] X. Yan, J. Wei, J. Guo, C. Hua, J. Liu, L. Chen, L. Hei, C. Li, Mechanism of graphitization and optical degradation of CVD diamond films by rapid heating treatment, Diam. Relat. Mater. 73 (2017) 39–46, https://doi.org/10.1016/j.diamond.2016.11.010.
[42] J. Qian, C. Pantea, G. Voronin, T.W. Zerda, Partial graphitization of diamond crystals under high-pressure and high-temperature conditions, J. Appl. Phys. 90 (2001) 1632–1637, https://doi.org/10.1063/1.1382832.
[43] V.N. Strekalov, V.I. Konov, V.V. Kononenko, S.M. Pimenov, Early stages of laser graphitization of diamond, Appl. Phys. Mater. Sci. Process 76 (2003) 603–607, https://doi.org/10.1007/s00339-002-2014-3.
[44] V. n. Strekalov, Graphitization of diamond stimulated by electron-hole recombination, Appl. Phys. A 80 (2005) 1061–1066, https://doi.org/10.1007/s00339-003-2362-7.
[45] Q. Nian, Y. Wang, Y. Yang, J. Li, M.Y. Zhang, J. Shao, L. Tang, G.J. Cheng, Direct laser writing of nanodiamond films from graphite under ambient conditions, Sci. Rep. 4 (2014) 1–8, https://doi.org/10.1038/srep06612.
[46] E.M. Baitinger, E. a. Belenkov, M.M. Brzhezinskaya, V. a. Greshnyakov, Specific features of the structure of detonation nanodiamonds from results of electron microscopy investigations, Phys. Solid State 54 (2012) 1715–1722, https://doi.org/10.1134/S1063783412080057.
[47] J. Hu, P. Yang, C. Lieber, Nitrogen-driven sp3 to sp2 transformation in carbon nitride materials, Phys. Rev. B 57 (1998) R3185–R3188, https://doi.org/10.1103/PhysRevB.57.R3185.
[48] V.A. Greshnyakov, E.A. Belenkov, Investigation on structural transitions of graphenes into diamond polymorphs at high pressure, J. Phys. Conf. Ser. 1124 (2018), 022002, https://doi.org/10.1088/1742-6596/1124/2/022002.